DOI: 10.21062/mft.2026.030 http://www.journalmt.com

Applications of the Boriding Process in the Defence Industry

Martin Jaššo (0009-0007-6142-7808)[1], Richard Pastirčák (0000-0002-6944-4959)[2], Peter Fabian (0000-0001-9371-3998)[2], Jozef Bronček (0000-0002-6934-0383)[3]
[1]HS Technik. Žilinská cesta 84, 013 11, Lietavská Lúčka. Slovak Republic. E-mail: jasso.martin@hstechnik.sk
[2]Faculty of Technological Engineering, University of Žilina. Univerzitná 8215/1, 010 26 Žilina. Slovak Republic E-mail: richard.pastircak@fstroj.uniza.sk; peter.fabian@fstroj.uniza.sk
[3]Department of Design and Mechanical Elements, University of Žilina. Univerzitná 8215/1, 010 26 Žilina. Slovak Republic. E-mail: jozef.broncek@fstroj.uniza.sk

The study analyses current trends in the manufacturing of highly stressed components used in the defence industry, with a particular focus on handgun components. These parts are commonly produced from low-alloy steels that are refined to achieve medium strength levels. To enhance their resistance to mechanical and thermal loading, conventional production routes typically involve surface hardening followed by tempering. This study investigates the potential of replacing these established methods with a chemical–thermal surface treatment, specifically boriding, in which the surface layer is enriched with boron atoms. The mechanical properties of selected materials used for test samples are described and compared after treatment by induction surface hardening and boriding. The results provide a basis for evaluating the applicability of boriding as an alternative surface treatment for highly stressed components in the defence industry.

Keywords: Handgun barrel, Surface treatment, Induction hardening, Boron surface saturation

1 Introduction

Every manufacturer of components for the defence industry possesses its own know-how regarding the processes and materials used in the production of its products. At the same time, the end users impose different requirements on the final quality and performance of these components. Among the most widely manufactured products of the defence industry are handguns, primarily because they are extensively used not only in the defence sector but also in the civilian sphere. In the context of handguns, the most critical and at the same time historically oldest component is the barrel (Fig. 1). Within the barrel, phenomena occur that belong to the most extreme processes of classical physics. These include the action of extremely high pressures and elevated temperatures generated by the explosion of the propellant charge, as well as intensive friction. Friction arises both between the projectile (Fig. 2) and the inner surface of the barrel and between the outer surface of the barrel and the breech mechanism in which the barrel is mounted. For these reasons, strict requirements are imposed on both the base material of the barrel and its subsequent surface treatment, which must ensure sufficient strength, wear resistance, and long-term durability under severe operating conditions [1].

In the defence industry, barrels for handguns are commonly manufactured from low-alloy steels that have been quenched and tempered. However, in practice, other types of materials may also be encountered, such as various aluminium alloys or composite materials, depending on the specific application. In the case of steel barrels, grades such as 42CrMo4 or 30CrV9 are predominantly used in a quenched and tempered condition to a medium strength level, due to their excellent toughness, which enhances resistance to pressure loading [2,3]. The tensile strength of these materials typically ranges from approximately 1000 to 1200 MPa. To increase resistance to friction and wear, induction surface hardening is commonly applied. Due to differences in chemical composition and carbon (C) content, these materials exhibit different achievable surface hardness values, ranging from about 50 HRC for 30CrV9 to up to 60 HRC for 42CrMo4. Regarding heat resistance, both materials can withstand the temperature of approximately 580 °C, and the applied surface treatment does not significantly affect this temperature resistance [3,4,5].

During the boriding process, boron atoms diffuse into the lattice of the base metal, leading to the formation of a hard interstitial boride compound on the surface of the component. The resulting boride layer may consist of a single-phase or a dual-phase structure, typically composed of FeB and Fe_2B, which exhibit significantly higher hardness than conventionally hardened, nitrided, or carburized layers. The formed boride layers provide high

resistance to high-temperature oxidation up to approximately 850 °C, as well as enhanced resistance to abrasive and corrosive environments, including acidic and alkaline solutions, sodium chloride, and similar media [6,7].

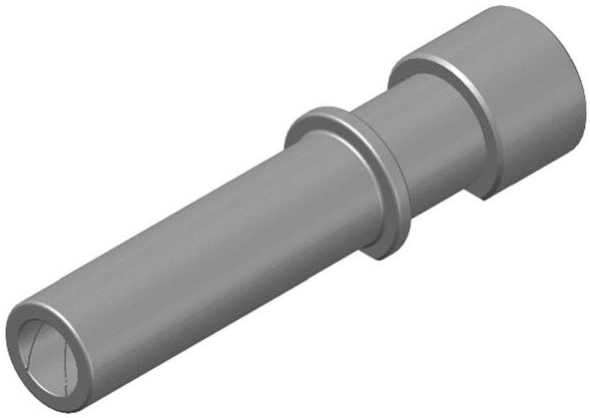

Fig. 1 *Model of a handgun barrel*

Boriding is still regarded as one of the non-conventional methods of chemical–thermal treatment. Active boron is generated in a saturated environment at a high boron concentration and at elevated temperatures, typically around 1000 °C, depending on the material used. Surface saturation with boron atoms can be carried out using several techniques, including gaseous boriding, boriding in molten salt baths, with or without the application of an electrolytic process, as well as powder boriding [7].

Powder boriding offers advantages because it can be applied using a straightforward procedure and at relatively low cost compared with other boriding methods. In this surface saturation method, a refractory container is filled with the boriding agent in powder form, and the samples are embedded within it. After the boriding process, the container is allowed to cool to room temperature, and the residual powder is removed from the surface of the samples. However, in powder boriding, it is essential to define the process parameters influencing the kinetics of boron diffusion to achieve optimal layer properties [8,9].

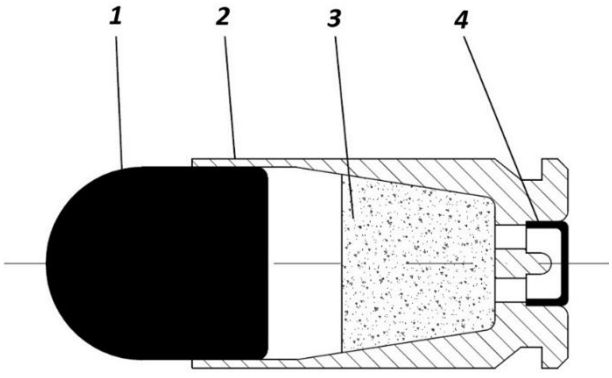

Fig. 2 *Bullet used in handguns: 1–steel bullet, 2–brass case, 3–propellant charge, 4–primer.*

The application and development of boriding remain an active area of research, with new possibilities for its usage continuing to emerge. Diffusion boriding represents a promising approach, as it can significantly extend the life of components and broaden the range of applications of structural materials. Boriding enhances resistance to wear under abrasive friction conditions, including at elevated temperatures. It is therefore considered an effective surface hardening technology for steels, enabling hardness values of up to approximately 2000 HV to be achieved [10,11].

Data reported in the literature regarding the microhardness of the Fe_2B phase show some variability. The microhardness of the FeB phase typically ranges from 1800 to 2200 HV, with alloying elements and carbon (C) content exerting a measurable influence on the hardness of this phase. In contrast, the hardness of the Fe_2B layer is not affected by carbon content or alloying elements, and the hardness of borides is also independent of subsequent heat treatment. This indicates that, following boriding, the properties of the base material can be modified without compromising the integrity of the borided layer [12].

The properties of the base material after boriding are not described in detail in the available literature. However, it can be inferred that they depend significantly on the chemical composition of the steel and on any subsequent heat treatment applied after the boriding process. The thickness of the diffusion layer formed during boriding typically ranges from 0.1 to 0.3 mm, with a layer thickness of approximately 0.2 mm considered optimal for industrial applications. The solubility of carbon in boride phases is very low (less than 0.047% C). During the growth of boride crystals from the surface toward the core, carbon diffuses into the core, resulting in an increased carbon concentration beneath the boride layer. As a result of the substitution of carbon by boron in the diffusion zone, the carbon content immediately below the boride layer may increase to near-eutectoid level, even in low-carbon steels [13,14,15].

Chemical elements such as molybdenum (Mo), tungsten (W), and chromium (Cr) slow the growth of the boride layer while simultaneously suppressing the formation of the characteristic saw-tooth morphology of the FeB phase. As a result, the final layer thickness is lower than that observed in unalloyed carbon steels. This phenomenon is associated with the diffusion of these elements from the boride layer toward the core of the material. Simultaneously, alloying elements such as nickel (Ni), manganese (Mn), and silicon (Si) diffuse in the opposite direction, from the core toward the surface. Since silicon and carbon are insoluble in the boride layer, they are displaced into the region beneath it, within the base matrix. This process results in

the formation of a transition zone, or intermediate layer, with a hardness of approximately 300 HV. This zone develops between the core and the surface layer, particularly in steels containing approximately 1 % silicon [16,17,18].

The development of technologies for producing boride layers represents a fundamental prerequisite for their successful and broader industrial application. Boriding provides significantly higher wear resistance than carburized, nitrided, or electroplated chromium layers. In carburization, a gradual transition between the hardened surface layer and the softer core is required after quenching. In nitriding, the diffusion zone plays a critical role in determining the performance of the treated material. By contrast, in boriding, the functional performance is governed primarily by the properties of the surface boride layer [18].

The fundamental principle of boriding lies in the diffusion of a foreign element, specifically boron, into the surface of a metallic component. This diffusion process enables the achievement of a desirable combination of mechanical and functional properties. In austenitic steels, the resulting surface layer is predominantly composed of the FeB phase, while intergranular regions are filled with boride compounds. However, this microstructural configuration leads to reduced adhesion of the boride layer. As a result, under dynamic or impact loading conditions, partial delamination of the hard surface layer may occur [19,20].

Boriding can be applied to most ferrous materials, except for aluminium and silicon steels. Applicable materials include structural steels, carburized, quenched, tool steels, stainless steels, cast steels, air-hardened steels, malleable, and sintered steels. In addition, boriding can be performed on other materials, such as nickel-, cobalt-, and molybdenum-based alloys. Nickel-based alloys can be borided without a reduction in corrosion resistance, while simultaneously producing a hard surface with exceptional wear resistance [21].

Borided components are used in a wide range of industries, including the oil and gas sector, agricultural machinery, and the automotive industry. In addition, certain tools used for pressing, textile processing, and extrusion or injection molding are also treated using this method. Typical components on which boride layers are applied include valve components (such as guides, seats, stems, and control valves), pump components (including impeller housings, casings, pistons, and cylinders), and, in agricultural machinery, cutting and harvesting attachments for combines, separators, crop transport mechanisms, and cutting elements. In the automotive industry, examples include oil pumps and gears for diesel engines, among others [22,23].

This study focuses on strategies for enhancing the mechanical and tribological properties of handgun barrels, with a particular emphasis on improving the wear resistance of their surface layers. Deformation or damage to the barrel results in a deterioration of handgun functionality and, in many cases, necessitates its replacement. Such replacements are not only time-consuming but also require significant logistical resources, making the extension of barrel life a critical consideration [23]. In the experimental section, we present and evaluate the results of selected tests performed on surface-hardened and borided samples. All experiments were conducted under controlled laboratory conditions and supervised by qualified personnel to ensure accuracy and reproducibility.

2 Materials and methods

Two materials commonly used in the manufacture of handgun barrels were selected for this study. These materials are also widely used in mechanical engineering for components subjected to high levels of mechanical loading. One of the selected materials was 42CrMo4 steel, intended for quenching and tempering as well as surface hardening, and commonly used in the production of highly stressed machine components and road motor vehicle parts, where high strength and toughness are required, particularly for shafts and fastening elements.

In terms of chemical composition, this material is a low-alloy, high-quality chromium–molybdenum steel containing 0.38–0.45% carbon (C), 0.50–0.80% manganese (Mn), 0.17–0.37% silicon (Si), 0.90–1.20% chromium (Cr), up to 0.50% nickel (Ni), 0.15–0.30% molybdenum (Mo), and a maximum of 0.035% phosphorus (P) and sulphur (S) (Tab. 1). The material was supplied in a quenched and tempered condition corresponding to a medium strength level, with an average tensile strength of approximately 1100 MPa. This condition reflects the typical state in which the material is used for the manufacture of handgun barrels.

The second investigated material was 30CrV9 steel, which is intended for quenching and tempering, surface hardening, and chemical–thermal treatment. In practical applications, it is used for the manufacture of highly stressed quenched and tempered machine components, including nitrided gears. Due to its high hardenability, this steel is also suitable for larger forgings. With respect to its chemical composition, this material can be classified as a low-alloy, high-quality chromium–vanadium steel containing 0.24–0.34% carbon (C), 0.40–0.80% manganese (Mn), 0.17–0.37% silicon (Si), 2.20–2.50% chromium (Cr), 0.10–0.20% vanadium (V), and a maximum of 0.035% phosphorus (P) and sulphur (S) (Tab. 1).

Tab. 1 *Chemical composition of selected materials*

Chemical composition	C [wt %]	Mn [wt %]	Si [wt %]	Cr [wt %]	Mo [wt %]	Ni [wt %]	V [wt %]	P [wt %]	S [wt %]
42CrMo4	0.38 - 0.45	0.50 - 0.80	0.17 - 0.37	0.90 - 1.20	0.15 - 0.30	max. 0.50	x	max. 0.35	max. 0.035
30CrV9	0.24 - 0.34	0.40 - 0.80	0.17 - 0.37	2.20 - 2.50	x	x	0.10 - 0.20	max. 0.35	max. 0.035

Samples were produced from the above-mentioned materials for subsequent experimental testing, including static tensile, impact bending, tribological, dimensional stability, and barrel tests (Fig. 3).

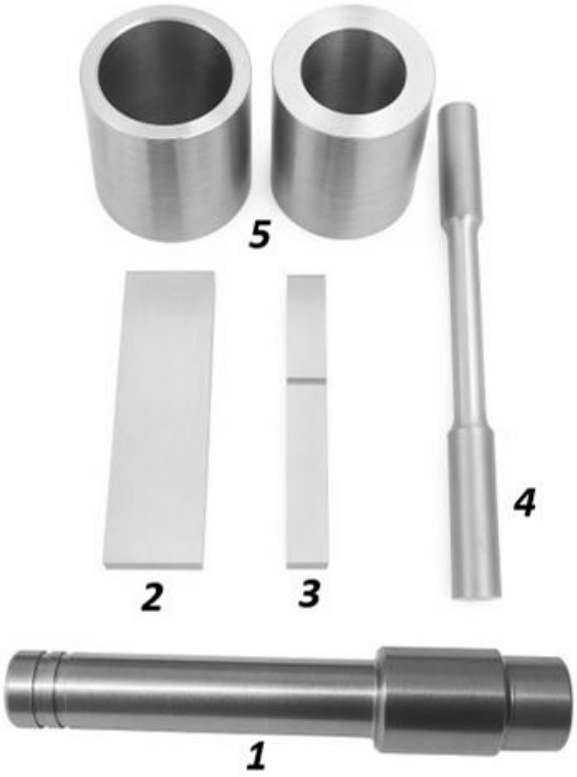

Fig. 3 *Types of samples manufactured for the experiment: 1–barrel sample, 2–sample for the Ball-on-Flat test, 3–sample for the impact bending test, 4–sample for the static tensile test, 5–sample for the dimensional stability test*

2.1 Induction Hardening

Induction surface hardening was performed on all sample types using a VM500 machine (EFD Induction S.A., Germany). This equipment operates on the principle of high-frequency electromagnetic waves generated by the power source, enabling the formation of a hardened layer with a thickness ranging from 0.5 to 1.5 mm, depending on the capacitor configuration. This process is characterised by a hardening temperature approximately 50–80 °C higher than that used in conventional bulk quenching in a furnace. The elevated temperature results from the immediate cooling of the hardened zone behind the inductor, which significantly affects heat distribution within the component's surface and is important for achieving the desired microstructure.

A cooling medium composed of 92% demineralized water and 8% aquatenside was used during the process. The main process parameters were as follows:

- machine power of 42 kW,
- generator frequency of 167 kHz,
- voltage of 133 V,
- current of 31 A,
- and a square-coil inductor.

The hardening temperature was maintained between 880 and 900 °C, with an initial soaking time of 0.6 s at this temperature. The inductor moved along the longitudinal axis of the sample at a feed rate of 1100 mm/min, followed by immediate cooling using the aquatenside–demineralized water solution applied as a spray (Fig. 4). The cooling medium was maintained at 18 °C. During induction hardening, the samples were tempered in a furnace at 150 °C, with a 60-minute heating ramp followed by an equal soaking period at the target temperature.

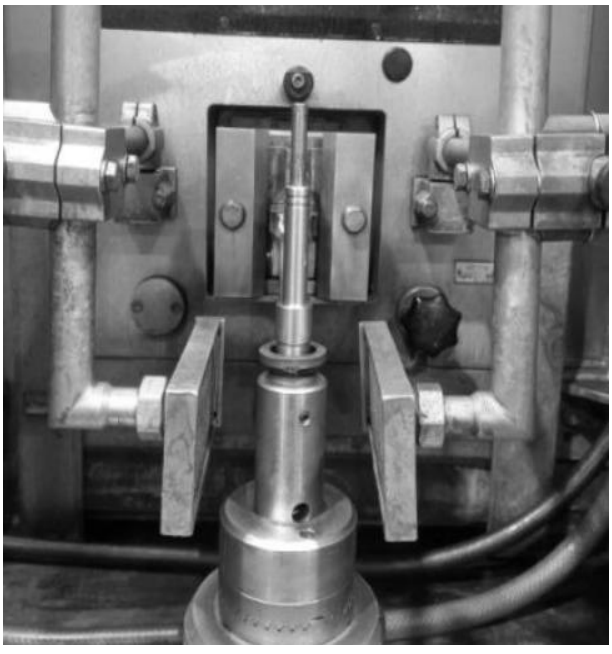

Fig. 4 *Induction surface hardening of a barrel sample*

2.2 Boriding

For the experiment, surface saturation with boron atoms using a powder mixture was selected as the boriding method. The aim was to produce a layer with an optimal arrangement of boride phases while simultaneously achieving the highest mechanical performance. The boriding powder DURFERIT DURBORID G was used, and the process was conducted in an electric resistance furnace.

The samples were placed sequentially in the container in layers, ensuring that they did not touch each other and that the gaps between them were adequately filled with boriding powder. The process parameters were as follows (Fig. 5):

- preheating the furnace to 600 °C,
- inserting the container into the furnace,
- controlled heating to 900 °C,
- soaking temperature for 5 hours,
- removing the container from the furnace,
- allowing the container to cool naturally,
- extracting samples after reaching a temperature of 20 °C.

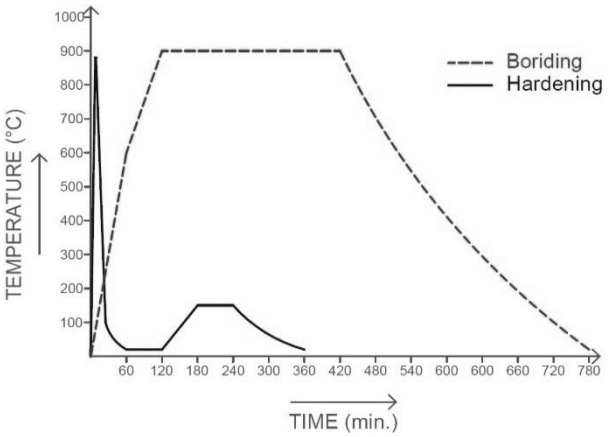

Fig. 5 *Comparison of temperature versus time during induction surface hardening and boriding*

2.3 Mechanical Testing – Static Tensile Test and Impact Bending Test

The static tensile test was conducted on an INSTRON universal testing machine in accordance with EN ISO 6892-1. Samples with a circular cross-section and a gauge diameter (b_0) of 8 mm were used. The reference temperature for both the samples and the surrounding environment was maintained at 20 °C. The tensile test aimed to determine the following material properties: tensile strength (R_m), elongation (A), reduction of area (Z), and modulus of elasticity (E). Two samples were tested for each combination of material and surface treatment.

The impact bending test was performed using a Charpy testing machine in accordance with EN ISO 148-1. Square cross-section samples with a U-shaped notch were used, and the reference temperature was also 20 °C. Two samples for each material and processing method were tested. The purpose of this test was to determine the impact toughness coefficient K_{CU}.

2.4 Microstructure and microhardness

Microhardness tests are essential to complement the mechanical properties obtained from tensile and impact bending tests. The measured microhardness, however, is also strongly influenced by the microstructure, the distribution of individual phases, and the grain size of the structural components.

The material microstructure, and consequently the resulting mechanical properties, are influenced by several factors, including chemical composition, manufacturing route, post-production processing (e.g., drawing or rolling), heat treatment procedures (such as quenching and tempering), and additional thermal or chemical–thermal processes designed to tailor specific material properties.

The samples used for microscopic observations were also employed for microhardness measurements. Before testing, the samples were prepared by standard wet metallographic procedures. Following mechanical preparation, the surfaces were etched in a 5% Nital solution to reveal the phases formed within the material matrix. Microscopic observations were performed using a Neophot 32 optical metallographic microscope at a magnification of 800×. The primary aim of these observations was to verify the formation of the intended microstructure in the surface layers after induction hardening and boriding. In the case of boriding, particular attention was paid to the presence and distribution of both boride phases, as well as to confirming that the selected technological parameters, specifically temperature and process duration, were appropriate.

For samples of the base material and those subjected to induction surface hardening, several approaches to microhardness evaluation were available. However, the options were more limited for the borided samples. This limitation was due to the smaller thickness of the borided layer compared with the hardened layer, as well as the anticipated higher hardness and the need to determine the microhardness of individual grains. For these reasons, the Hanemann method was selected for microhardness evaluation. The Hanemann microhardness tester, regarded as one of the most precise instruments of its type, is integrated into the Neophot 32 microscopic system. This tester employs a Vickers diamond indenter as the penetrating body, which is mounted directly within a special microscope objective.

Microhardness measurements were performed at a magnification of 256×, 50 μm below the sample surface, with individual measurement points spaced 50 μm apart. Due to differences in layer thickness, 10 measurement points were evaluated for the borided samples, while a higher number of measurements was obtained for the induction-hardened samples. An indenter load (P) of 40 g was applied. The measured parameter was the diagonal length of the indentation (u), which was subsequently converted into the microhardness value HVm using equation (1).

$$HVm = \frac{1855\,P}{u^2}\ [g.mm^{-2}] \quad (1)$$

Where:
P…Applied load [g],
u…Indentation diagonal [mm].

2.5 Tribological Test – Ball-on-Flat

The ability of a material to withstand friction over extended periods is an essential property for selecting materials for handgun barrel applications. To evaluate the coefficient of friction (μ) of thermally and chemically treated samples, the Ball-on-Flat tribological test was used.

The test principle involves pressing a stationary counterbody (ball) against a flat sample, after which the ball moves linearly across the sample surface under a predefined normal load and for a specified duration. The test was conducted in accordance with ASTM G99, using one sample for each surface treatment. Throughout the experiments, a reference temperature of 20 °C and a relative humidity of 50% were maintained. The test aimed to evaluate the shape and extent of surface damage (wear track) produced by the ball on the sample surface.

For the test, a hardened ball made of high-carbon, chromium-alloyed bearing steel (100Cr6) with a diameter of 2 mm was used. A normal load of 10 N (≈ 1020 g) was applied to the ball. The test was conducted over a duration of 18000 s (≈ 5 h), with a sliding speed ranging from 0 to 20 mm·s^{-1}. The test was performed under dry friction conditions, without the use of any lubricant.

The flat sample over which the ball slid had dimensions of 60 × 20 mm (A × B) and a thickness of 5 mm. Following manufacturing and grinding, the samples exhibited surface roughness values of Ra 0.236 μm for 42CrMo4 samples and Ra 0.116 μm for 30CrV9 samples. Surface roughness measurements were carried out using a MAHR MarSurf PS10 device, with an evaluation length (ln) of 4 mm and a basic cut-off length (lr) of 0.8 mm. The measurements were processed using a Gaussian filter.

2.6 Dimensional Stability Test

The final test performed on the samples involved evaluating dimensional changes following chemical–thermal treatment. As noted earlier, induction surface hardening is currently the most commonly used method for this type of component, producing a hardened layer with a thickness of 0.7–1.0 mm. For barrels with a wall thickness of approximately 4.0 mm at their narrowest section, this hardened layer results in negligible deformation of the bore. Since the external dimensions of the barrel are generally non-critical, induction hardening is typically performed at the final stage of the manufacturing process, followed only by blackening. It should be noted that machining of the barrel bore is not feasible after induction surface hardening, making the control of dimensional changes during the process particularly important.

In the case of boriding, protecting the internal surfaces of the barrel from boron saturation is difficult to achieve. In certain applications, however, a harder barrel bore may be desirable to enhance wear resistance and improve resistance to thermal shocks. Consequently, it is essential to evaluate dimensional changes after boriding, as the resulting borided layers are difficult to machine. The only practical tools for machining such surfaces are grinding wheels made of industrial diamond or cubic boron nitride (cBN). However, tools with an outer diameter of no more than 8 mm, suitable for this purpose, are currently not readily available.

For the experiment, two types of cylindrical samples were manufactured, representing the narrowest and thickest sections of a barrel. Each sample had a length of 50 mm, with wall thicknesses of 4 mm for the narrower cylinder and 8 mm for the thicker cylinder. During manufacturing, particular emphasis was placed on achieving the highest possible precision in the geometric parameters of both the external and internal surfaces (Fig. 6). The monitored parameters included cylindricity, runout, and surface roughness, with a target roughness of Ra 0.8 μm, corresponding to the standard used in actual barrel production. All geometric and surface specifications were met in accordance with the technical drawings.

The dimensions of the samples were measured both before and after the boriding surface treatment. In each case, the samples were tempered at a measurement temperature of 20 °C for 48 hours. Temperature monitoring was carried out using the sensor of the coordinate measuring machine.

The dimensional measurements were conducted in accordance with ISO 1101:2017 using a TIGO SF 3D coordinate measuring machine (Hexagon). The probing device featured a ruby sphere with

a diameter of 3 mm. Samples were positioned at the center of the machine's chuck to ensure measurement repeatability. The machine was calibrated before testing, achieving a maximum measurement deviation of 1 μm. The probe applied the contact force of 0.12 N. Surface scanning was performed at a speed of 10 mm·s^{-1}, with a pitch of 4 mm per rotation. Measurement data were recorded in protocols and subsequently analyzed in the results section of this study.

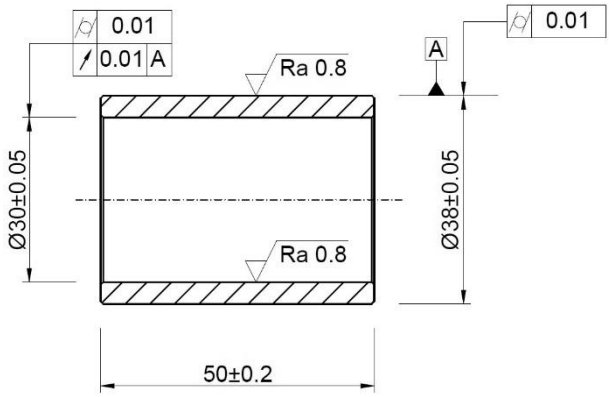

Fig. 6 *Requirements for sample production for dimensional stability tests*

3 Discussion of results

The results of the experiment concern the technological properties of the materials after treatment, which directly impact the life of the final product. In addition to the intrinsic mechanical properties, economic and environmental aspects of the individual processes represent crucial considerations.

When comparing boriding, nitriding, cementation followed by quenching, and induction surface hardening, the latter emerges as the most cost-effective option. This advantage is primarily attributed to its short processing time, high repeatability, and ease of integration into existing production lines.

From an ecological perspective, induction hardening is also the least environmentally burdensome process. Unlike nitriding or cementation, it does not involve chemicals that require special storage or environmentally safe disposal. Additionally, the water-based quenching medium can be reused multiple times, significantly reducing both resource consumption and waste generation.

3.1 Microstructure and Microhardness

The steel used for samples can be characterized as a ferritic–pearlitic steel with a carbon content of up to 0.6%. As noted earlier, both materials were supplied in a heat-treated condition, exhibiting a medium tensile strength of approximately 1100 MPa, corresponding to a hardness of 360 HVm. The heat treatment significantly influences the base material's microstructure, resulting in refinement and the formation of a minor fraction of retained martensite.

For 42CrMo4 steel, the hardened layer thickness after induction surface hardening was determined to be 1.00 mm, using the conventional 500 HVm threshold to define the layer boundary. The surface layer exhibited a microhardness of 724 HVm. To ensure comparability with the borided samples and account for the size of the indentation, microhardness measurements were performed at a depth of 0.05 mm beneath the surface.

Metallographic evaluation revealed the formation of a martensite–troostite structure in the surface layer (Fig. 7). However, this structure is not entirely optimal in terms of grain fineness and phase distribution homogeneity. The observed enlargement of martensite and troostite grains indicates that the material experienced significant overheating during induction heating, resulting in coarsening of the austenite grains. Induction surface hardening is characterized by an extremely high heating rate, which limits the time available for diffusion processes in austenite, followed by rapid cooling that constrains the martensitic transformation. The combination of these factors results in a coarser martensitic morphology and partial formation of troostite in the transition zone.

For 30CrV9 steel, the thickness of the hardened layer after induction surface hardening was measured at 1.00 mm, using the conventional 500 HVm threshold to define the layer boundary. This measurement is consistent with that obtained for the other steel tested. Experimental results indicate that the differing chemical compositions of the two steels did not substantially influence hardenability, as nearly identical hardened layer depths were obtained under identical induction hardening conditions.

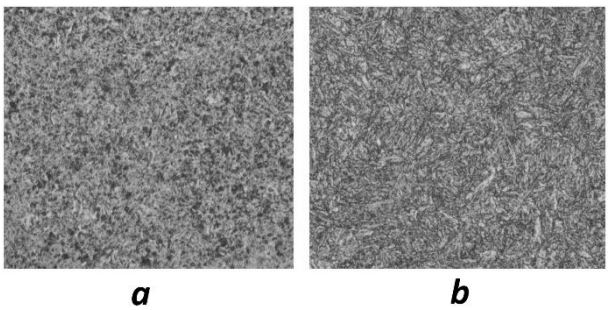

Fig. 7 *Microstructure of 42CrMo4 steel after induction surface hardening (800× magnification); a) hardened layer, b) base material*

Nevertheless, 30CrV9 steel exhibited lower microhardness values. At a depth of 0.05 mm below the surface, the microhardness measured 608 HVm. This difference is primarily attributed to the chemical

composition, particularly the lower carbon content (≈ 0.3 %), which critically influences the maximum hardness achievable after martensitic transformation. The final hardness is also affected by the chromium content, which increases the austenitization temperature. Since 30CrV9 contains a higher chromium content (approximately 2 % Cr), this can result in a slightly different microstructure under identical heat treatment conditions.

Metallographic evaluation confirmed the formation of a fine martensitic structure in 30CrV9 steel (Fig. 8), with martensite grains noticeably smaller than those observed in 42CrMo4 steel. The finer martensitic morphology can be attributed to the lower carbon content, the higher heating rate, and the limited diffusion during induction hardening. The core hardness remained comparable for both materials, at approximately 370 HVm, corresponding to the medium-strength tempered condition of the base material.

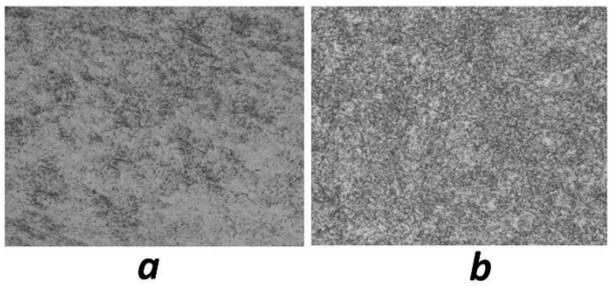

Fig. 8 *Microstructure of 30CrV9 steel after induction surface hardening (800× magnification); a) hardened layer, b) base material*

The samples subjected to boriding exhibited a significantly higher surface hardness compared with those treated by induction surface hardening, despite the resulting diffusion layer being thinner. However, it is important to note that the boriding process required a duration several times longer than that of the induction hardening treatment.

While induction hardening primarily involves martensitic transformation and the associated changes and densification of the crystallographic lattice, boriding is a diffusion-driven process in which boron atoms penetrate the material's surface layer. During this process, boron forms hard intermetallic phases with iron (FeB and Fe_2B) while displacing certain elements with higher atomic mass or lower affinity for boride formation, such as carbon. For comparison, the atomic mass of boron is 10.811 $g \cdot mol^{-1}$, whereas that of carbon is 12.011 $g \cdot mol^{-1}$.

Directly beneath the borided layer, a transition zone develops in which material impurities, such as silicon (Si) and copper (Cu), become locally concentrated. This region is characterized by significantly lower hardness, resulting from the redistribution of alloying elements during the diffusion saturation process and the formation of a transition layer beneath the borides.

Samples of 42CrMo4 steel reached a surface microhardness of 1377 HVm after boriding, measured at a depth of 0.05 mm below the surface. The total thickness of the diffusion layer was approximately 75 μm. Based on these measurements, it can be concluded that the FeB phase predominated in the borided layer. In contrast, the Fe_2B phase either did not form or developed as an extremely thin layer, insufficient for reliable detection at the measured depth. This behaviour is typical for steels with higher carbon content and for cases in which the surface region exhibits a high boron concentration, as the formation of FeB suppresses the development of the inner Fe_2B layer.

At a depth of approximately 0.10 mm below the surface, a transition layer was observed, with a measured hardness of 298 HVm. In the subsequent measurement points within the substrate, hardness values ranged from 310 to 330 HVm. These results indicate that the boriding process also affected the properties of the base material, causing a slight reduction in hardness compared with its initial state (Fig. 9). This decrease is attributed to the high processing temperature, which effectively induces soft annealing, combined with the redistribution of alloying elements during diffusion saturation and the formation of the transition zone, where local depletion of carbide-forming elements occurs.

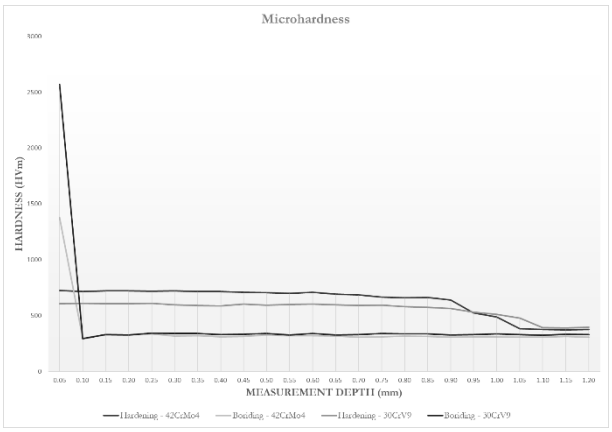

Fig. 9 *Microhardness distribution across the cross-section for all sample treatment methods*

Samples of 30CrV9 steel exhibited a significantly higher surface microhardness after boriding, reaching 2569 HVm, with a borided layer thickness of approximately 80 μm. Beneath the borided layer, at a depth of approximately 0.10 mm, a transition layer was observed, with a microhardness of 293 HVm. In subsequent measurement points within the substrate, the hardness stabilized between 330 and 340 HVm, indicating that, as with 42CrMo4 steel,

the core microstructure was affected by softening and redistribution of alloying elements during the diffusion saturation with boron.

From a metallographic perspective, the 30CrV9 samples exhibited a pronounced saw-tooth morphology of the borided layer (Fig. 10), characteristic of the combined formation of Fe_2B and FeB phases. The surface portion of the layer was predominantly composed of the Fe_2B phase, while beneath it, within the depletion layer, columnar FeB structures extended downward. This hierarchical structure is advantageous, as it enhances adhesion to the substrate, reduces the risk of delamination, and improves resistance to cracking and localized spalling. A similar morphology was observed in the 42CrMo4 samples, although to a significantly lesser extent (Fig. 11).

The measured microhardness values (Fig. 12) clearly demonstrate that, despite identical boriding process parameters, the resulting layer hardnesses differed between the two steels. These differences can be attributed to their chemical compositions. The higher carbon and molybdenum content in 42CrMo4 steel slows the growth of boride phases and limits layer thickness. In contrast, 30CrV9 steel, with lower carbon content and the presence of vanadium, facilitates more intensive boron diffusion into the surface, leading to the formation of a combined FeB + Fe2B layer and resulting in significantly higher microhardness.

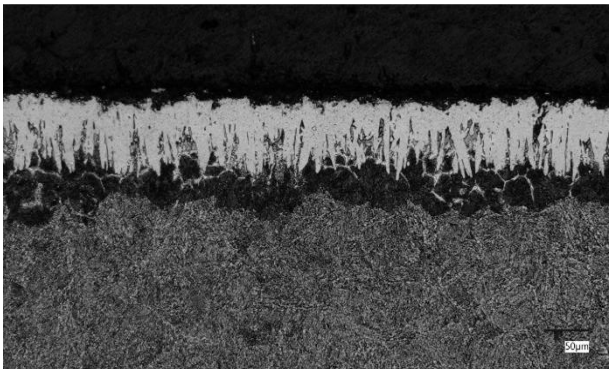

Fig. 10 *Microstructure of 30CrV9 steel after boriding*

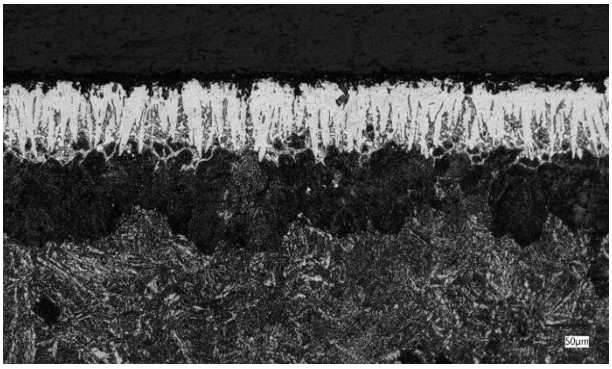

Fig. 11 *Microstructure of 42CrMo4 steel after boriding*

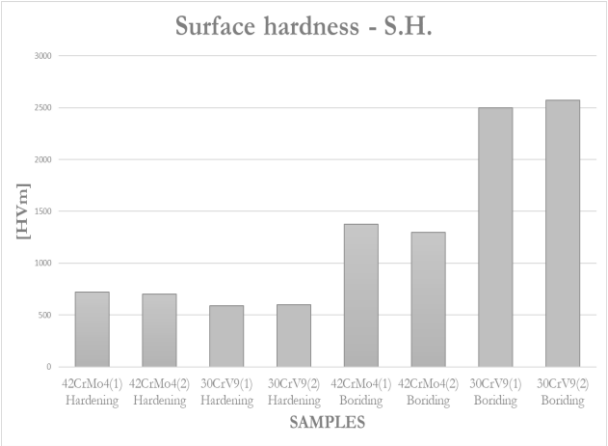

Fig. 12 *Comparison of surface hardness (S.H.) for selected treatment methods*

3.2 Static Tensile Test

The static tensile test was conducted to determine the fundamental material properties, including tensile strength (R_m), modulus of elasticity (E), elongation (A), and reduction of area (Z). Microhardness measurements and metallographic analysis confirmed that the boriding process had a significant impact on the properties of the base material.

Samples of 42CrMo4 steel subjected to induction surface hardening exhibited tensile strengths (R_m) in the range of 1248–1297 MPa, elongation (A) of 3–4%, and reduction of area (Z) of 30–37%. In contrast, the same material after boriding displayed a lower tensile strength of 786–798 MPa. Ductility, however, improved significantly, with elongation reaching 12–13% while the reduction of area remained at 37%. These results indicate that, while boriding decreases overall strength due to the transition layer and changes in the core microstructure, it simultaneously enhances elastic–plastic performance. This behaviour can be attributed to the considerably thinner hardened layer relative to induction hardening.

For 30CrV9 steel samples subjected to induction surface hardening, the tensile strength (R_m) ranged from 1360 to 1405 MPa, elongation (A) was 5–6%, and reduction of area (Z) was 24–26%. Following boriding, the samples exhibited a tensile strength of 1289–1314 MPa, elongation of 6–7%, and an unchanged reduction of area (24–26%). These results suggest that the effect of boriding on the strength of 30CrV9 steel is less significant than in 42CrMo4 steel. This behaviour can be attributed to differences in chemical composition and the more favourable morphology of the boride layer in 30CrV9. Nevertheless, the higher intrinsic strength of 30CrV9 is associated with comparatively inferior elastic–plastic properties relative to 42CrMo4.

The graph comparing tensile strength (R_m) clearly demonstrates that induction-hardened samples

achieved higher tensile strength than borided samples for both materials (Fig. 13). Although boriding produces a tough surface layer, it also changes the core microstructure, resulting in a reduction in the overall strength of the samples.

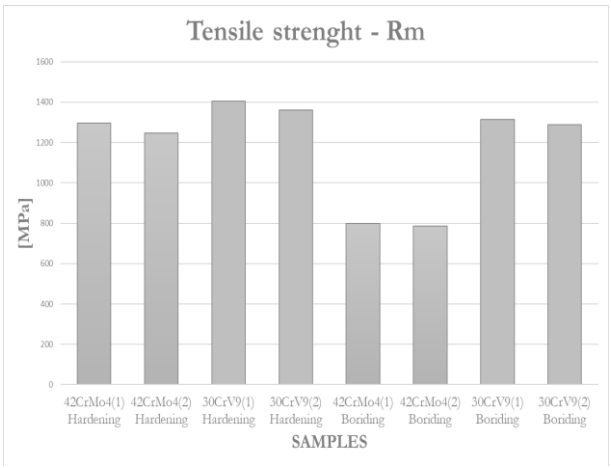

Fig. 13 *Comparison of tensile strength (R_m) for selected treatment methods*

The borided samples demonstrated a greater capacity for plastic deformation in both types of steel, as reflected by the increased elongation values (A) (Fig. 14). This behaviour can be attributed to the reduced thickness of the hardened layer combined with simultaneous modifications in the core material properties induced by the diffusion process. The effect is particularly significant in 42CrMo4 steel.

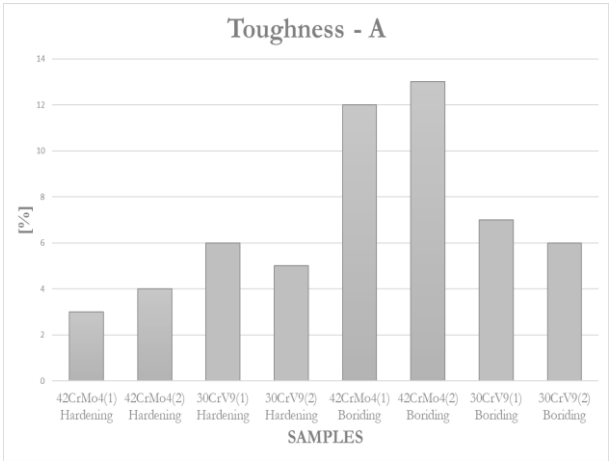

Fig. 14 *Comparison of toughness (A) for selected treatment methods*

Observation and analysis of the reduction of area (Z) revealed no significant differences between the two processing methods (Fig. 15). In the borided samples, the material's ability to localize deformation up to fracture was comparable to, or slightly greater than, that of the induction-hardened samples, reflecting the enhanced elastic–plastic properties imparted by boriding.

Fig. 15 *Comparison of the reduction of area (Z) for selected treatment methods*

3.3 Impact bending test

42CrMo4 steel samples subjected to induction surface hardening exhibited a toughness coefficient (K_{CU}) of 55–56 J/cm². After boriding, the same material displayed significantly lower K_{CU} values, ranging from 15 to 23 J/cm² (Fig. 16).

Induction-hardened samples of 30CrV9 steel exhibited a toughness coefficient (K_{CU}) of 100–105 J/cm², closely matching the values of the base material. This confirms that the core remained essentially unaffected during induction hardening, while the surface hardness achieved was the lowest among all tested conditions (608 HV_m). In contrast, borided samples of the same steel showed a drastic reduction in K_{CU}, with values of only 14–15 J/cm² (Fig. 16). This significant decrease reflects the limited plastic deformability of the borided layer, composed of FeB and Fe_2B borides. It also demonstrates that the extreme surface hardness is attained at the expense of toughness.

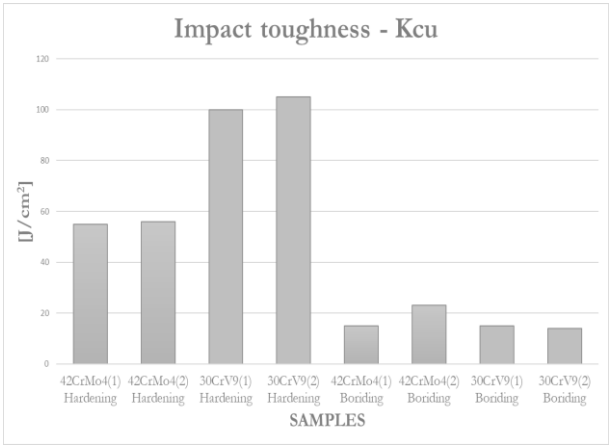

Fig. 16 *Comparison of impact toughness coefficient (K_{CU}) for selected treatment methods*

Compared with induction-hardened samples, borided samples exhibited significantly lower toughness values (K_{CU}). This reduction is attributable

not only to the presence of an extremely hard but brittle boride layer (FeB/Fe_2B), but also to the influence of the prolonged boriding process on the base material. In contrast, the highest K_{CU} values were observed in 30CrV9 samples after induction hardening, where the original tough matrix was preserved, and the surface layer remained the least hard and brittle.

The test results indicate that boriding reduces the toughness of both materials examined.

3.4 Tribological test – Ball-on-Flat

During the Ball-on-Flat tribological test, the coefficient of friction (μ) was evaluated for the borided samples. For comparison, the friction coefficients of the surface-hardened samples were taken as μ = 0.50 (–) for 42CrMo4 and μ = 0.52 (–) for 30CrV9.

During the Ball-on-Flat test, two characteristic zones of the friction curve were considered. The first, the run-in zone, extends from the start of the test until the coefficient of friction reaches its maximum. The second, the stabilized zone, is where the friction coefficient behaviour over time is evaluated. As shown in Fig. 17, 42CrMo4 performed better in the first zone, reaching a maximum friction coefficient of μ = 0.85 (–) at approximately 300 s. In contrast, 30CrV9 exhibited a slower run-in, but achieved a lower friction coefficient in the second zone, around μ = 0.80 (–), indicating superior long-term tribological performance after boriding.

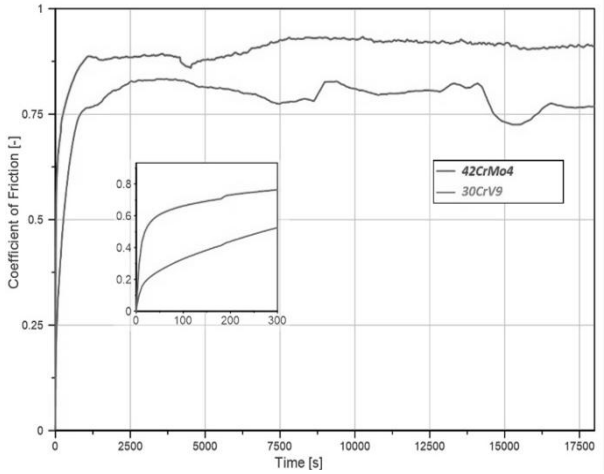

Fig. 17 *Comparison of impact toughness coefficient (K_{CU}) for selected treatment methods*

During the test, an unusual phenomenon was observed. At the contact point between the hardened steel ball and the sample surface, no typical wear groove formed on the sample; instead, the ball itself was damaged, exhibiting abrasion and localized surface flattening (Fig. 18). This behaviour is attributed to the extremely high hardness of the borided layers, which significantly exceeds that of the steel ball. Consequently, the current test results cannot be considered fully reliable. For an objective comparison, the experiment should be repeated using a ceramic ball or another material with higher surface hardness.

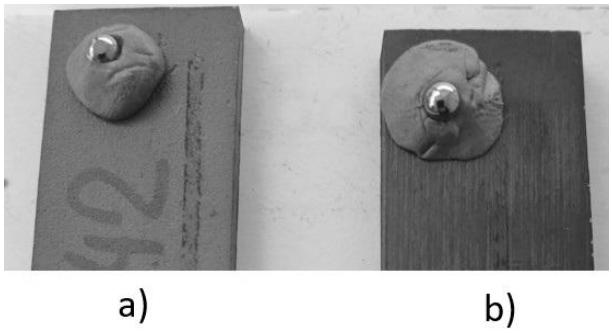

Fig. 18 *Surfaces of samples and balls after Ball-on-Flat testing; a) sample from 42CrMo4 steel, b) sample from 30CrV9 steel.*

3.5 Dimensional Stability Test

The tests aimed at assessing dimensional changes after processing were conducted exclusively on borided samples. From a technological perspective, preventing saturation of the inner surface during boriding is particularly challenging. In the case of handgun barrels, however, it is often desirable for the bore to become harder and more resistant to wear and thermal shocks. Consequently, it was necessary to measure the dimensional and geometric changes that occurred in the inner bore of the samples following the boriding process.

During the tests, the following parameters were monitored:

- changes in the outer diameter of the sample ($d \rightarrow d_1$),
- changes in the inner diameter ($D \rightarrow D_1$),
- cylindricity of the inner surface (/O/),
- runout (↗) of the inner surface (D) relative to the outer surface (d).

For samples with a wall thickness of 8 mm, no significant dimensional or geometric changes were observed. Boriding, therefore, does not pose a technological risk at this wall thickness.

For samples with a wall thickness of 4 mm, more significant changes were observed. For samples made from 42CrMo4 steel, the following measurements were recorded:

- outer diameter: increased from d = 38.035 mm to d_1 = 38.054 mm (+0.019 mm),
- inner diameter: increased from D = 29.970 mm to D_1 = 29.973 mm (+0.003 mm).

The most significant issue was the change in the geometry of the inner surface:

- cylindricity increased from /O/ = 0.003 mm to /O/ = 0.021 mm,
- runout between the inner and outer surfaces increased from ↗ = 0.005 mm to ↗ = 0.027 mm.

The surface roughness also increased slightly due to boriding. Before the process, roughness values ranged from Ra = 0.396 to 0.632 μm, whereas after boriding they increased to Ra = 0.548–0.827 μm. Fig. 19 illustrates the change in the shape of the inner surface of the sample, measured before and after the boriding process.

The sample made from 30CrV9 steel showed even more significant geometrical changes after boriding. Before boriding, the measured outer and inner diameters were:

- outer diameter: d = 38.041 mm,
- inner diameter: D = 29.967 mm.

After boriding, the dimensions changed to:

- outer diameter: d_1 = 38.054 mm (increase of 0.013 mm),
- inner diameter: D_1 = 29.956 mm (decrease of 0.011 mm).

It is important to note that the evaluation was based on the average of all measurement points, rather than the maximum circumscribed or minimum inscribed diameters. While the average dimensions did not exhibit dramatic changes, significant geometrical deviations were observed:

- cylindricity of the inner surface increased from /O/ = 0.002 mm to /O/ = 0.038 mm,
- runout increased from ↗ = 0.003 mm to ↗ = 0.043 mm.

The more significant deformation observed in 30CrV9 indicates that this steel is more sensitive to dimensional changes during boriding compared to 42CrMo4. The resulting change in shape is illustrated in Fig. 20.

Additionally, the surface roughness increased, ranging from Ra = 0.461–0.592 μm before boriding to Ra = 0.494–0.801 μm after the process.

The measurement results demonstrated that the boriding process induces measurable changes in sample dimensions, surface roughness, and geometric accuracy. The magnitude of these changes strongly depends on wall thickness and chemical composition, with more significant deformations observed in 30CrV9 steel. This material appears to be more sensitive to volumetric changes and internal stresses generated during boron diffusion.

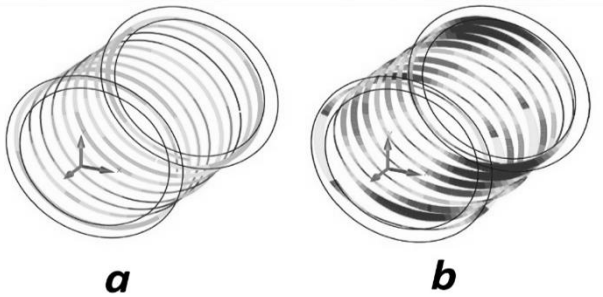

Fig. 19 *Comparison of inner diameter geometry of a 42CrMo4 sample; a) before boriding, b) after boriding.*

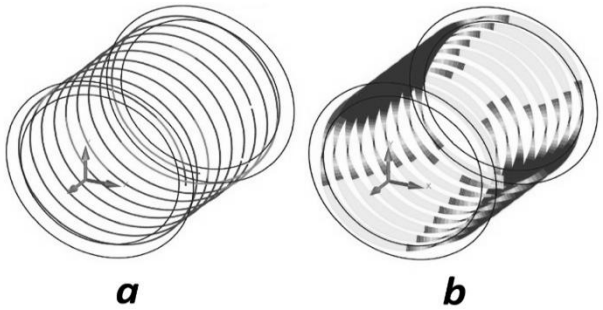

Fig. 20 *Comparison of inner diameter geometry of a 30CrV9 sample; a) before boriding, b) after boriding.*

In all cases, an increase in surface roughness was observed, which is a typical manifestation of the growth of FeB and Fe_2B borides in the surface layer of the material. The obtained results demonstrate that boriding significantly affects dimensional and shape accuracy in thin-walled components, which may represent a technological limitation when applying this process to handgun barrels.

A comprehensive summary of the experimental results is presented in Tab. 2.

Tab. 2 *Summary and comparison of experimental results*

MATERIAL PROPERTY	STEEL - 42CrMo4		STEEL - 30CrV9	
	Surface hardening	Boriding	Surface hardening	Boriding
Microhardness	724 HVm	1377 HVm	608 HVm	2569 HVm
Thickness of layer	1.000 mm	0.075 mm	1.000 mm	0.080 mm
Influence of base material	none	partially annealed	none	partially annealed
Tensile strength (Rm)	1297 MPa	798 MPa	1405 MPa	1314 MPa
Toughness (A)	3-4 %	12-13 %	5-6 %	6-7 %
Reduction of area (Z)	30-37 %	37%	24-26 %	24-26 %
Impact toughness (K_{CU})	55-56 J/cm²	15-23 J/cm²	100-105 J/cm²	14-15 J/cm²
Coefficient of friction (μ)	0.50	0.85	0.52	0.80
Dimensional changes	minimal	medium	minimal	significant

4 Conclusion

This experiment aimed to determine whether the traditional induction surface hardening process used in the defence industry can be replaced by boriding to improve the functional and mechanical properties of components exposed to high friction, mechanical loading, and elevated service temperatures. To address this aim, test samples were produced from two low-alloy carbon steels commonly used in highly stressed components, 42CrMo4 and 30CrV9. Each material was subjected to both induction surface hardening and boriding, followed by a comprehensive set of mechanical, tribological, and metallographic analyses to evaluate and compare the effects of the applied surface treatment technologies.

The experimental results demonstrated that boriding produced a hard diffusion layer composed of FeB and Fe_2B borides on the surfaces of both investigated materials, with the character and thickness of this layer being strongly dependent on the chemical composition of the steel. Steel 30CrV9 exhibited a substantially higher surface microhardness, reaching up to 2569 HVm, together with a well-developed saw-tooth boride layer morphology, indicating more favourable boron diffusion under the selected process parameters. In contrast, 42CrMo4 steel achieved a lower surface microhardness of 1377 HVm, and the formation of a continuous Fe_2B sublayer was likely incomplete. This behaviour can be attributed to the higher carbon and molybdenum contents in 42CrMo4 steel, which retard boron diffusion and restrict the growth of boride phases.

It was also demonstrated that the high processing temperature and prolonged duration of boriding significantly affected the core material of both steels. A transition zone formed directly beneath the borided layer, characterized by reduced hardness and localized changes in chemical composition, including carbon depletion and the accumulation of impurity elements. This phenomenon had a directly negative effect on tensile strength and impact toughness, as both investigated materials exhibited decreases in ultimate tensile strength (R_m) and impact toughness (K_{CU}) after boriding. Conversely, because the borided samples possess a thin surface layer with high hardness, they demonstrated improved elastic–plastic behaviour, as indicated by higher elongation and reduction of area, compared with induction surface-hardened samples.

Tribological testing confirmed that the borided layer substantially improves frictional resistance. In the steady-state regime, 30CrV9 steel exhibited a lower coefficient of friction ($\mu \approx 0.80$), indicating favourable tribological performance.

During the test, however, wear occurred on the hardened steel ball rather than on the sample surface, reflecting the extremely high hardness of the borided layer. This observation also indicates that the steel ball used is not fully suitable for testing such highly hardened surfaces. For future experiments, it is therefore recommended to use a ceramic or carbide ball to obtain more reliable and representative tribological results.

A particularly noteworthy finding was the dimensional and geometric changes observed after boriding, particularly in samples with a wall thickness of 4 mm. Deviations in cylindricity, roundness, and surface roughness were noted for both materials, with the deformations being more significant in 30CrV9 steel. These results highlight a significant technological limitation, as machining the borided layer is extremely challenging. In thin-walled components, such as handgun barrels, such deformations can lead to unacceptable changes in the internal geometry. However, the boriding process also offers significant advantages. The borided layer can withstand subsequent heat treatment without risk of degradation, providing the opportunity to optimize the mechanical properties of the core through additional hardening after boriding. This combined approach could potentially eliminate the reduction in strength and toughness observed in the present experiment.

Based on the conducted tests, it can be concluded that boriding offers significant potential for enhancing surface hardness and tribological performance. However, its application in thin-walled components is limited by dimensional and geometric distortions. For 42CrMo4 steel, adjustments to the process temperature and duration may be necessary to achieve a fully developed borided layer. For 30CrV9 steel, further analysis of the boriding effect on dimensional stability across different wall thicknesses is recommended.

In the future, it is recommended to extend the experiment by:

- optimizing the boriding process parameters, including temperature, duration, and powder activation,
- conducting subsequent heat treatment of the borided samples,
- using harder tribological counterparts in Ball-on-Flat tests,
- and studying stress fields during boron diffusion and their impact on the deformation of thin-walled components.

The comprehensive results of this study indicate that boriding can be an attractive alternative for improving the durability of components in

the defence industry. However, its implementation in the production of critical components requires further optimization and a detailed evaluation of its effects on dimensional stability and component life.

References

[1] VILIŠ, J., VÍTEK, R., ZOUHAR, J., STEJSKAL, J., NEUMANN, V. (2023). Experimental Investigation of Armour (Armox-Aramid-UHMWPE). In: *Manufacturing Technology*, Vol. 23, No.6, pp. 935-948. DOI: 10.21062/mft.2023.083.

[2] KILIC, A., KARTAL, G., URGEN, M., TIMUR, S. (2013). Effects of electrochemical boriding process parameters on the formation of titanium borides. In: *Surface Engineering and Applied Electrochemistry*, Vol. 49, No. 2, pp. 168–175. DOI: 10.3103/S1068375513020051.

[3] ZIMMERMAN, C., BUGLIARELLO-WONDRICH, N. (2014). Deep case boriding for extreme wear resistance. In: *HTPRO*, Vol. 2, No. 4, pp. 9–11.

[4] RUDNEV, V., LOVELESS, D., COOK, R. (2017). *Handbook of Induction Heating*. CRC Press, Boca Raton. ISBN 978-1-138-74874-3.

[5] SVOBODA, P., JOPEK, M. (2024). The Effect of Strain Rate on the Friction Coefficient. In: *Manufacturing Technology*, Vol. 24, No. 2, pp. 289–293. DOI: 10.21062/mft.2024.027

[6] FISCHER-CRIPPS, A. (2004). *Nanoindentation*. Springer-Verlag, New York. ISBN 0-387-22045-3.

[7] MAJERÍK, J., MAJERSKÝ, J., BARÉNYI, I., CHOCHLÍKOVÁ, H., ESCHEROVÁ, J., KUBASÁKOVÁ, M. (2023). Surface Roughness, Topography, Accuracy, Chip Formation Analysis & Investigation of M390 and M398 Steels after Hard Machining. In: *Manufacturing Technology*, Vol. 23, No. 10, pp. 60–72. DOI: 10.21062/mft.2023.015

[8] ASKELAND, D. R., PHULÉ, P. P. (2001). *The Science and Engineering of Materials*. Thomson Learning, Belmont. ISBN 0-534-95373-5.

[9] POKLUDA, J., KROUPA, F., OBRDŽÁLEK, L. (1994). *Mechanické vlastnosti a struktura pevných látek: kovy–keramika–plasty*. PC-DIR, Brno. ISBN 80-214-0575-9.

[10] ENVER, A., UMUT, Y. (2003). The effects of conventional heat treatment and boronizing on abrasive wear and corrosion of SAE 1010, SAE 1040, D2 and 304 steels. In: *Tribology International*, Vol. 36, pp. 155–161. DOI: 10.1016/S0301-679X(02)00069-5.

[11] MECIT, Ö., YILMAZ, K., TUBA, O. (2023). Effect of boriding on high temperature tribological behavior of CoCrMo alloy. In: *Tribology International*, Vol. 187, Article 108697. DOI: 10.1016/j.triboint.2023.108697.

[12] SADUMAN, S., UGUR, S., CUMA, B. (2005). An approach to kinetic study of borided steels. In: *Surface and Coatings Technology*, Vol. 191, pp. 274–285. DOI: 10.1016/j.surfcoat.2004.03.040.

[13] RESÉNDIZ-CALDERÓN, C. D., CAMPOS-SILVA, I., SORIANO-VARGAS, O. (2025). Tribological performance of borided tool steel with minimum bio-lubrication for sheet metal forming applications. In: *Wear*, Vol. 566–567, Article 205748. DOI: 10.1016/j.wear.2025.205748.

[14] KEDDAM, M., CHENTOUF, S. M. (2005). A diffusion model for describing the bilayer growth (FeB/Fe_2B) during the iron powder-pack boriding. In: *Applied Surface Science*, Vol. 252, pp. 393–399. DOI: 10.1016/j.apsusc.2005.01.016.

[15] KANTORÍKOVÁ, E., MORAVEC, J., BIŇASOVÁ, V. (2023). The effect of borides on the mechanical properties of tool steels and sintered carbides. In: *Transportation Research Procedia*, Vol. 74, pp. 522–529. DOI: 10.1016/j.trpro.2023.11.177.

[16] CAMPOS, I., PALOMAR, M., AMADOR, A., MARTINEZ, J. (2006). Evaluation of the corrosion resistance of iron boride coatings obtained by paste boriding process. In: *Surface and Coatings Technology,* Vol. 201, pp. 2438–2442. DOI: 10.1016/j.surfcoat.2006.04.017.

[17] CAMPOS-SILVA, I., HERNÁNDEZ-SÁNCHEZ, E. (2001). Indentation size effect on the Fe_2B/substrate interface. In: *Surface and Coatings Technology*, Vol. 206, pp. 1816–1823. DOI: 10.1016/j.surfcoat.2011.07.029.

[18] CAMPOS, I., OSEGUERA, J., GARCÍA, J. A. (2003). Kinetic study of boron diffusion in the paste-boriding process. In: *Materials Science and Engineering*, Vol. 352, pp. 261–265. DOI: 10.1016/S0921-5093(02)00910-3.

[19] CULHA, O., TOPARLI, M., SAHIN, S. (2008). Characterization and determination of Fe_xB layers' mechanical properties. In: *Journal of Materials Processing Technology*, Vol. 206, pp. 231–240. DOI: 10.1016/j.jmatprotec.2007.12.020.

[20] VERMA, P. CH., MISHRA, S. K. (2020). Synthesis of iron boride powder by carbothermic reduction method. In: *Materials Today: Proceedings*, Vol. 28, pp. 902–906. DOI: 10.1016/j.matpr.2019.12.321.

[21] NOVÝ, F., HARVANEC, J., MIČIAN, M. (2024). The influence of induction hardening, nitriding and boronising on the mechanical properties of conventional and sintered steels. In: *Coatings*, Vol. 14, No. 12, Article 1602. DOI: 10.3390/coatings14121602.

[22] XIAOXIAO, L., LIU, W., YUAN, J. (2025). The influence of an alternating current field on pack boriding for medium carbon steel at moderate temperature. In: *Coatings*, Vol. 15, Article 39. DOI: 10.3390/coatings15010039.

[23] CALIK, A., UCAR, N., KARAKAS, N. S. (2019). Pack-boriding of pure iron with powder mixtures containing ZrB_2. In: *High Temperature Materials and Processes*, Vol. 38, pp. 342–346. DOI: 10.1515/htmp-2017-0081.